Sigma Journal of Engineering and Natural Sciences
Web page info: https://sigma.yildiz.edu.tr
DOI: 10.14744/sigma.2025.00172

Research Article

SCAPS-1D performance analysis of $MAPbI_3$ and $MASnI_3$ based perovskite solar cells

Velpuri LEELADEVI[1], Piyush KUCHHAL[1], Debasis DE[2]

[1]*Department of Electrical and Electronics, School of Engineering, UPES, Dehradun, 248007, India*
[2]*Energy Institute Bengaluru (EIB), Centre of Rajiv Gandhi Institute of Petroleum Technology (RGIPT), 560064, India*

ARTICLE INFO

Article history
Received: 01 August 2024
Revised: 11 November 2024
Accepted: 21 April 2025

Keywords:
ETL; HTL; $MAPbI_3$; $MASnI_3$; Perovskite Solar Cells; SCAPS 1D; Simulation

ABSTRACT

In this study, the performance of two perovskite solar cells (PSCs) devices that are based on methylammonium tin (II) iodide ($MASnI_3$) and methylammonium lead iodide ($MAPbI_3$) as absorber materials are investigated and optimized. This work helps in the advancement of sustainable energy technologies by balancing the lead-free stability of $MASnI_3$ and the high efficiency of $MAPbI_3$. The Solar Cell Capacitance Simulator in One Dimension (SCAPS 1-D) was used to examine the impact of a thickness difference in the layer on power conversion efficiency (PCE) and other parameters that are linked to performance. The results clearly show that $MASnI_3$ manages to deliver a 12% PCE with an open-circuit voltage (V_{oc}) of 0.7945 V, while $MAPbI_3$ obtains a PCE of 18.41% and V_{oc} of 1.4742 V, thus establishing the efficiency difference between the two materials. Nevertheless, as $MASnI_3$ has the upper hand when it comes to its stability, the lead-free solution is more plausible. The research reports conducted in this study have allowed for the identification of the methodology of assessing bandgap alignment and material selection to improve the performance of $MASnI_3$, which further presents the possibilities of new technologies that operate without lead. These results indicate the importance of PSC to the sustainability and scalability of energy solutions.

Cite this article as: Leeladevi V, Kuchhal P, De D. SCAPS-1D performance analysis of $MAPbI_3$ and $MASnI_3$ based perovskite solar cells. Sigma J Eng Nat Sci 2026;44(5):3492–3502.

INTRODUCTION

The main energy source has been fossil fuels, which are increasingly unsustainable due to rising global energy demand, limited natural availability, and considerable environmental impacts. Therefore, there has been a more intensified global transition towards clean and renewable energy sources. One of the promising technologies is Photovoltaic (PV) energy source due to its scalability and abundance. PV cells convert light energy directly into electricity via photochemical processes.

Among the technologies that have emerged in recent times related to PV, perovskite solar cells (PSCs) have significant attention based on their remarkable power conversion efficiency (PCE), surpassing 27% in single junction configurations [1, 2]. This makes PSCs an alternative technology with prospects of outperforming the traditional

*Corresponding author.
*E-mail address: leeladevivelpuri1999@gmail.com

This paper was recommended for publication in revised form by Editor-in-Chief Ahmet Selim Dalkilic

Published by Yıldız Technical University Press, İstanbul, Turkey
© Author. This is an open access article under the CC BY-NC license (http://creativecommons.org/licenses/by-nc/4.0/).

silicon-based solar cells in any future scenario [3]. The exceptional optical and electrical properties of perovskite material are found as an explanation for the success of PSCs, that can absorb light over a wide range, extending from the visible to near-infrared wavelengths. However, PSCs suffer major setbacks such as poor material stability under ambient conditions, and environmental and health hazards because of toxic constituents [4].

ABX_3 perovskite structure is the key to PSC functionality: its composition is varied, where "A" can be a monovalent cation, such as Formamidinium, $NH_2CHNH_2^+$, or Methylammonium, $CH_3NH_3^+$, "B"-divalent metal, such as lead, Pb^{2+}, and "X"-halide ion, such as iodine, I^-, or bromine, Br^-. To date, the optimal combination for high-performance PSCs includes Formamidinium or Methylammonium at the A-site, lead at the B-site, and iodine or bromine at the X-site [5]. A conventional PSC configuration consists of six individual layers as shown in Figure 1: layer (1), a hole transport layer (HTL), typically Spiro-OMeTAD, which promotes hole extraction; layer (2), an electron transport layer (ETL), typically titanium dioxide, TiO_2, which promotes electron extraction; Layer (3), the absorber layer (AL), typically methylammonium lead iodide ($MAPbI_3$), which is shown as the perovskite layer in Figure 1, absorbs light and generates charge carriers; layer (4) is a transparent conductive substrate, usually fluorine-doped tin oxide; layer (5) is a glass substrate to hold the structure upright, which supports structural stability; and layer (6) is a metal electrode, such as gold, Au, for charge collection [6].

Even though $MAPbI_3$ has been widely used as an AL due to its relative efficiency and accessible characteristics, its application is severely hindered by the toxicity of lead, a heavy metal that causes severe environmental and health consequences [7]. Lead contamination has the potential to leach into soil and water systems throughout the processes of manufacturing, usage, or disposal, presenting considerable ecological threats and enduring health risks. The limitations caused by these concerns hinder the scalability and commercial potential of $MAPbI_3$ -based solar cells, highlighting the urgent necessity to investigate lead-free alternatives. Research is ongoing to alleviate this issue by replacing lead with less toxic materials, such as Sn, thereby forming methylammonium tin iodide, $MASnI_3$. While $MASnI_3$ offers a lead-free solution, it introduces challenges such as higher instability, necessitating further research to enhance its stability and performance. Moreover, current HTL and ETL materials, such as Spiro-OMeTAD and TiO_2, also present limitations. Spiro-OMeTAD is expensive, hygroscopic, and requires dopants for improved conductivity, which compromises long-term device stability. TiO_2, on the other hand, demands high-temperature processing and is prone to degradation under ultraviolet light [8].

Several recent studies have explored strategies to optimize the PCE of $MASnI_3$, focusing on balancing defect density and doping concentration. This optimization enhances PCE by reducing recombination rates. For instance, a defect density of 10^{14} cm^{-3} and doping concentration of 10^{18} cm^{-3} demonstrated significant PCE improvement [9]. Similarly, the AL thickness plays a crucial role in PCE; an optimal thickness of 0.6 μm achieved a maximum PCE of 30.35% [10]. To achieve both high efficiency and stability, the choice of suitable ETLs and HTLs is critical. Research indicates that copper- and carbon-based ETLs and HTLs can significantly enhance PCE, achieving efficiencies as high as 25.18% [11]. Another study [12] identified ideal parameters for PCE improvement: an acceptor density of 2×10^{19} cm^{-3}, ETL thickness of 20 nm, AL thickness of 700 nm, and HTL thickness of 10 nm, which collectively increased efficiency from 11.89% to 23.84%.

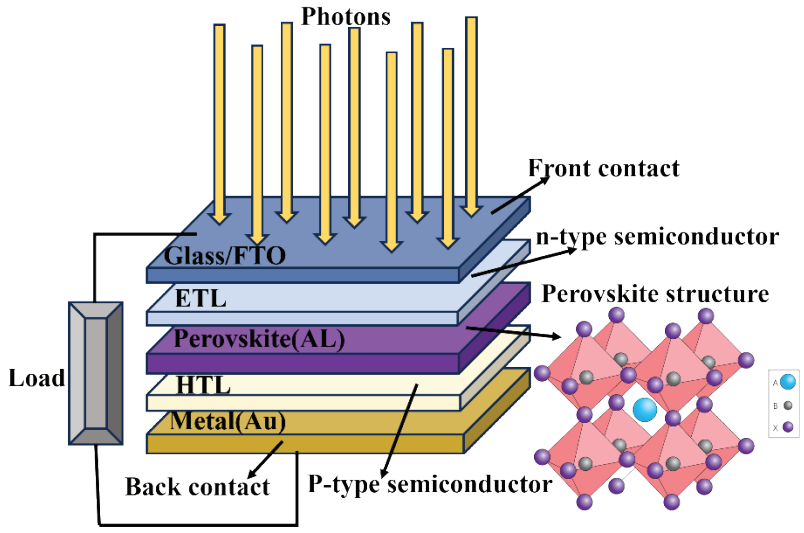

Figure 1. General configuration of perovskite solar cells.

Despite its promise, $MASnI_3$-based PSCs face stability challenges due to the oxidation of Sn (II) to Sn (IV), leading to increased defects and reduced performance [9]. Nevertheless, $MASnI_3$ offers a lead-free alternative with high PCE potential, stability against moisture and heat, and suitability for diverse applications, including buildings, vehicles, semi-transparent windows, and portable off-grid systems. Its low-cost manufacturing methods, such as solution processing, make this technology accessible for developing economies [13]. Furthermore, $MASnI_3$'s compatibility with tandem solar cells positions it as a promising candidate for next-generation photovoltaic systems [14, 15]. These advancements pave the way for hybrid modules designed for maximum energy yields, supporting global decarbonization efforts and providing cleaner alternatives to fossil fuels to meet the energy demands of both established and emerging markets.

In this study, we address the challenges associated with $MASnI_3$-based PSCs by integrating experimental data from existing literature with numerical simulations using the Solar Cell Capacitance Simulator (SCAPS-1D). Specifically, we compare and analyze key performance parameters of PSCs, such as short-circuit current density (J_{SC}), open-circuit voltage (V_{oc}), fill factor (FF), and PCE, for different device structures.

Through numerical simulations, we systematically optimized critical device parameters, including the thicknesses of the HTL, ETL, and AL, to identify configurations that maximize device performance. By varying these sensitive parameters, we investigated their impact on efficiency, stability, and overall performance. Additionally, we explored alternative materials for HTL and ETL layers, focusing on options that offer improved stability, cost-effectiveness, and scalability compared to conventional industry standards.

To provide a comprehensive understanding, Section 1.1 "perovskite structure" delves into the fundamental structure of perovskite materials, examining the influence of the Goldschmidt tolerance factor on crystal stability. Section 2 "materials and methods" presents the simulation and analysis methodology, emphasizing the role of three key differential equations in modeling PSC behavior. The SCAPS-1D simulator, widely used for PSC research, is introduced in Section 2.2 "input parameter and device structure", which also details the input parameters essential for accurate simulations. Finally, in Section 3, "result and discussion" we analyze the influence of AL, HTL, and ETL thickness variations on solar cell performance, presenting findings through a detailed discussion of results.

This integrated approach aims to address the persistent issues of stability and efficiency in $MASnI_3$-based PSCs, while also offering insights into practical design improvements and material choices for future photovoltaic technologies.

Perovskite Structure

Group of materials that has a crystal structure whose formula is ABX_3 at different transition states is called as perovskite where 'A' is an organic or inorganic cation with coordinate are in (0.0,0.0,0.0), 'B' is an inorganic cation with coordinate are in (0.5,0.5,0.5) and 'X' is halogen group with coordinate of (0.5,0.5,0) that is bonded with both 'A' and 'B' cation [16]. Usually, 'X' can be halogen or oxygen Halide perovskite can be divided into two different types such as, alkali halide-based perovskite and organic-inorganic halide-based perovskite. Whereas in organic-inorganic halide based perovskite contains organic monovalent cation for 'A' which are $CH_3NH_3^+$, $NH_2CHNH_2^+$,$CH_3CH_2NH_3^+$. similarly, alkali halide based perovskite contains monovalent cation ('A') which can be Cs^+, Rb^+ and etc., for 'B' (divalent cation) which are usually Pb^{+2}, Ge^{+2}, Sn^{+2} and for 'X'(halogen anions) that are Cl^-, Br^-. F^-, I^- [17]. For octahedral and cubic octahedral geometries, we required cations 'A' and 'B' coordinates should be with 12 and 6 'X' anions. Few advantages for halide based perovskite has good electrical, magnetic and optical properties which are used in field of solar cell [18]. We can see an ideal structure for perovskite with cubic structure as shown in Figure 2.

The easiest way to picture a perovskite is as a big, positively charged atomic or molecular cation of type 'A' in the middle of a cube. The cube's edges are then filled with atoms 'B', which are also positively charged cations. The faces of the cube are filled with a smaller, negatively charged atom 'X'. The first PSC construction is based on the dye-sensitized solar cell, which has a layer of TiO_2 on top of which organic materials are deposited. In the PSC, the perovskite will only absorb light, but in the future, it will also work as a charge carrier to help electrons move around. For a perovskite structure to be solid, the size of each part needs to be carefully thought out. The Goldschmidt tolerance factor is used to figure out the crystal structure based on the ratio of the sizes of the ions (eq 1):

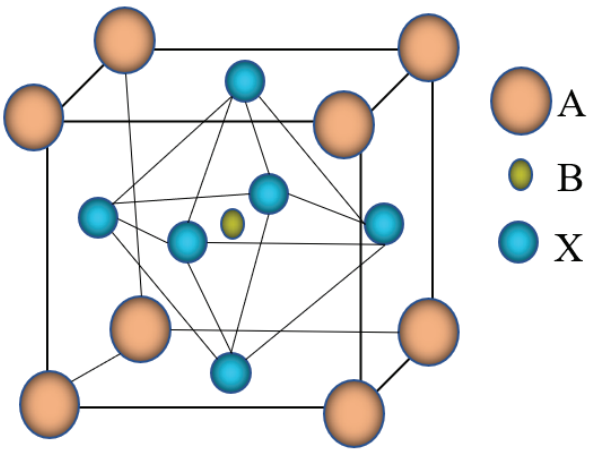

Figure 2. Structure of perovskite.

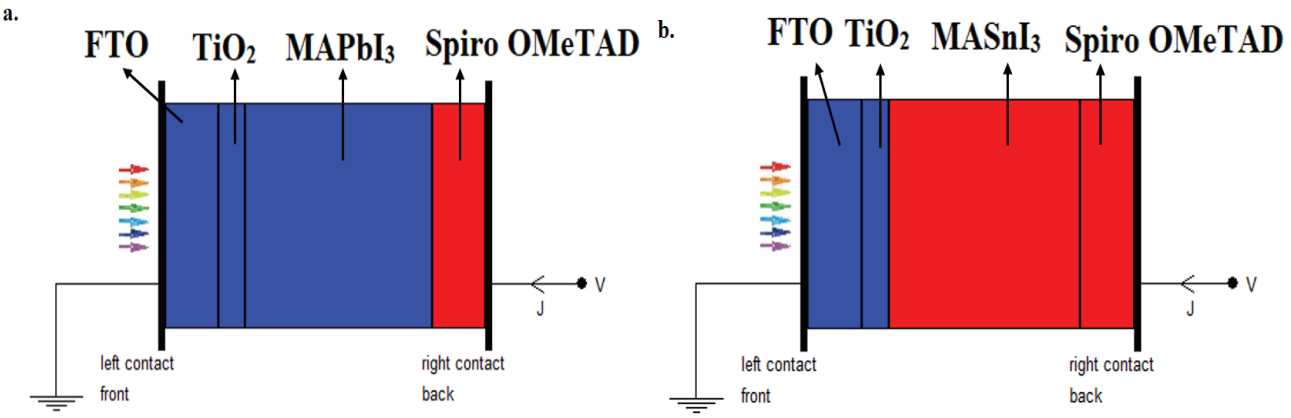

Figure 3. Model structure in SCAPS 1D a. $MAPbI_3$ b. $MASnI_3$.

$$t = \frac{rA + rx}{\sqrt{2}(rB + rx)} \quad (1)$$

Where rA, rB and rx are the ionic radii of 'A' site cation, 'B' site cation and 'C' site halide. When the tolerance factor is between 0.8 and 1, the perovskite can be held in place.

MATERIALS AND METHODS

Simulation is a key to understand how a solar cell device works physically as parameters changes with different conditions without actually wait for too long for results or spending money first. There are different types of modelling tools used for simulation, such as AMPS, MULTIPHYSICS,GPVDM,COMSOL,TCAD and SILVACO [19]. In this paper we will be using SCAPS 1D simulator for perovskite based solar cell. We can set up sever layer of semiconductor in SCAPS 1D simulator. As SCAPS 1D can be used for PSC mainly because it is very easy to use operation window with different models for defects, recombination, grading, generation.

Poisson and Continuity Equation

It is governing the electrical potential distribution inside PSCs. Given Poisson equation,

$$\frac{\partial}{\partial x}\left(\varepsilon(x)\frac{\partial \varphi}{\partial x}\right) = -q[p(x) - n(x) + N_D^+(x) - N_A^+(x) + p_t(x) - n_t(x)] \quad (2)$$

Similarly, for electrons and holes ensure the conservation of charge. Given continuity equation is,

$$\frac{\partial_{n,p}}{\partial x} = \frac{1}{q}\frac{\partial J_n}{\partial x} + (G_n - R_n) + \frac{1}{q}\frac{\partial J_p}{\partial x} + (G_p - R_p) \quad (3)$$

where, $\frac{\partial_{n,p}}{\partial x}$ concentration gradient of electron and hole, G and R generation and recombination rate of electron-hole pairs, N_A^+ and $N_D^+$are ionized acceptor and donor, p *and* n are density of free hole and electron, φ is an electrostatic potential, n_t and p_x are trapped density for electron and hole, q is elementary charge and ε is a permittivity.

Input Parameter and Device Structure

SCAPS 1D simulator to simulate $MASnI_3$ and $MAPbI_3$ based PSCs for the study of their performances. Below Figure 3. shows the structure of FTO/TiO_2/MA(Sn/Pb)I_3/Spiro OMeTAD which is used in experiment and the coloured arrows indicate direction of illumination of incident AM1.5G 1Sun spectrum.

Simulation was run twice for both FTO/TiO_2/$MASnI_3$/Spiro OMeTAD and FTO/TiO_2/$MAPbI_3$/Spiro OMeTAD model separately. the back metal contact which is gold (Au) with work function of 5.1eV and total defect density of p-type (N_t) is 1×10^{15} cm^{-3} for Spiro OMeTAD which acts as HTL. The heart of the device is the active layer, which is made up of $MAPbI_3$. It is also called the absorber layer [20, 21]. For Front metal contact which is TCO with work function of 4.4eV and total defect density of n-types (N_t) is 1×10^{15} cm^{-3} for TiO_2 which acts as ETL. The following Table 1 shows parameter settings for model FTO/TiO_2/$MAPbI_3$/Spiro OMeTAD. Simulation is performed under STC conditions with AM1.5G, 1000W/m^2, T = 300k whose cell properties like series resister (Rs) is 5.6Ωcm^2 and shunt resister (R_{sh}) is 4202Ωcm^2. To compare the performance of ETL, HTL and absorber layer by changing their thickness from 50 to 1000nm respectively to see their effect on overall performance of device [22-24]. However, for ETL and HTL can be as minimum as possible for better transfer of electrons and hole. But we have considered 50nm for ETL and 100nm for HTL as per experimental application. Table 2 shows properties of front, back metal contact and optical.

The equations used to calculate the output results (V_{oc}, J_{SC}, FF and PCE) of the device are defined as:

$$V_{oc} = \frac{nK_BT}{q}\left[\ln\left(\frac{I_L}{I_O} + 1\right)\right] \quad (4)$$

$$I_{SC} = I_L \quad (5)$$

Table 1. Parameter setting for model FTO/TiO_2/MA(Pb/Sn)I_3/Spiro OMeTAD [6]

PROPERTIES	FTO	TiO_2	$MAPbI_3$	$MASnI_3$	Spiro OMeTAD
t(nm)	100	50	50-1000	50-1000	100
E_g (eV)	3.5	3.3	1.55	1.3	2.9
χ (eV)	4	4.2	3.9	4.17	2.2
ε_r	9	10	30	6.5	3
N_C (cm^{-3})	2.2×10^{18}	2.5×10^{18}	2.2×10^{18}	1×10^{18}	2.5×10^{18}
N_V (cm^{-3})	1.8×10^{19}	1×10^{18}	1×10^{18}	1×10^{18}	1.8×10^{19}
V_n (cm/s)	10^7	10^7	10^7	1×10^7	10^7
V_P (cm/s)	10^7	10^7	10^7	1×10^7	10^7
μ_n (cm^2/Vs)	20	20	2.2	1.6	2×10^{-4}
μ_h (cm^2/Vs)	10	10	2.2	1.6	2×10^{-4}
N_A (cm^{-3})	20×10^{19}	10^{17}	9×10^{20}	0	0
N_D (cm^{-3})	0	0	0	1×10^{15}	1×10^{22}
N_t (cm^{-3})	1×10^{15}	10^{15}	8.5×10^{13}	2×10^{15}	1×10^{15}

Table 2. Back and front metal contact properties, optical properties [6]

Back metal contact properties	
Electron work function of Au	5.1eV
Surface recombination velocity of electron	10^5 cm/s
Surface recombination velocity of hole	10^7 cm/s
Front metal contact properties	
Electron work function of Transparent Conductive Oxide (TCO)	4.4eV
Surface recombination velocity of electron	10^5 cm/s
Surface recombination velocity of hole	10^7 cm/s
Optical filter	
Transmission mode	0.99

$$FF = \frac{J_{mp}\times V_{mp}}{J_{sc}\times v_{oc}} \quad (6)$$

$$PCE = \frac{V_{oc}\times J_{sc}\times FF}{P_{in}} \quad (7)$$

where, I_L and I_O are light generated current and reverse saturation current in solar cell, n is ideality factor and KBT/q is thermal voltage. Jmp, Vmp and P_{in} is current and voltage density at maximum power point and input power.

RESULTS AND DISCUSSION

Effect of Thickness in ETL, HTL and AL for Model FTO/TiO_2/$MAPbI_3$/Spiro OMeTAd

Simulation results for the PSC model which varying thickness of the ETL, HTL and AL materials by ranging from 50nm to 1000nm shown in Figure 4. As TiO_2 is most commonly used as ETL in PSC because of its high electron transfer efficiency and long-term stability in PSCs [25]. And has more effective photocatalytic activity, chemical stability, cheap cost, non-toxicity, and environmental friendliness, as well as superb optical and electrical features [26]. Spiro OMeTAD selected as HTL because of its simple implementation and high efficiency in organic-inorganic electronic devices [27].

By running simulation for each thickness to find out best thickness which it effects on overall performance of cell. The V-I curve and PCE curves, with each colour representing a distinct model thickness. Figure 4 and Table 3 demonstrate that the ideal AL thickness for $MAPbI_3$ was around 350 nm, at which point the PCE peaked at 18.41%. According to Figure 4(a), the PCE increased due to its capacity to capture photons, which enhances J_{SC} as more electron-hole pairs are generated. However, it subsequently declines due to the increased distance for carriers, raising the probability of recombination, which ultimately diminishes

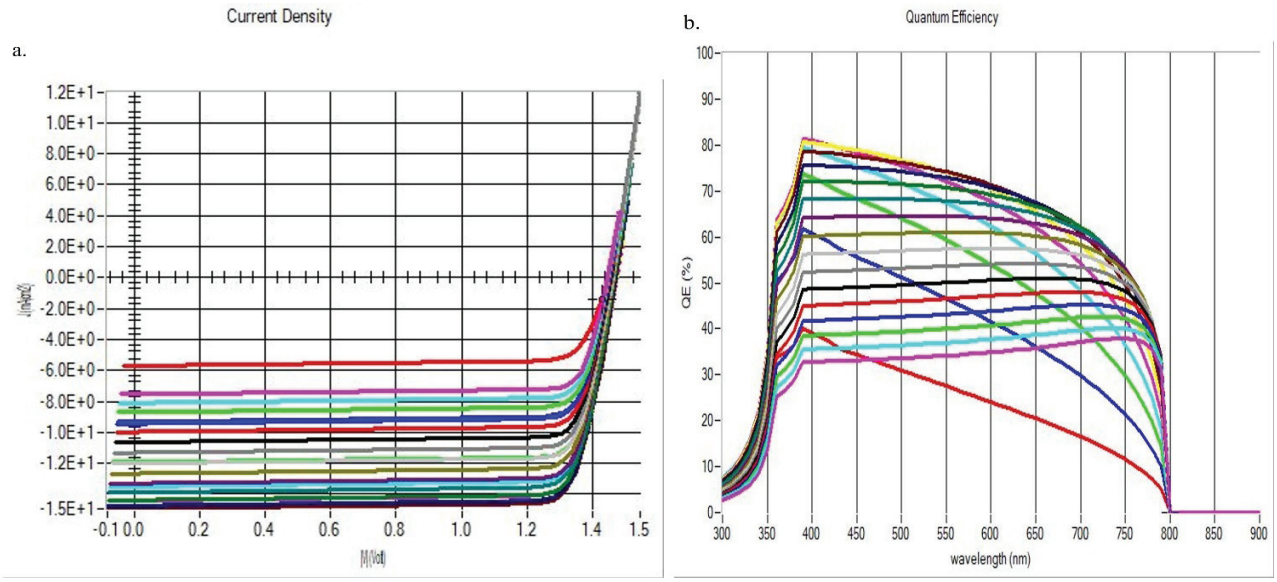

Figure 4. a. V-I curve and b. PCE curve for model FTO/TiO_2/$MAPbI_3$/Spiro OMeTAD (obtained from SCAPS 1D simulator) (each color indicates different thickness of AL red for 50nm to dark blue for 1000nm respectively).

Table 3. Simulation results for model FTO/TiO_2/$MAPbI_3$/Spiro OMeTAD(obtained from SCAPS 1D simulator)

t (nm)	V_{oc} (v)	J_{SC} (mA/cm²)	FF(%)	PCE(%)
50	1.4514	5.706	83.48	6.83
100	1.4693	9.439	83.67	11.61
150	1.4748	11.920	83.89	14.75
200	1.4763	13.496	83.79	16.69
250	1.4762	14.411	83.69	17.81
300	1.4754	14.843	83.66	18.32
350	1.4742	14.920	83.70	18.41
400	1.4726	14.74	83.78	18.19
450	1.4709	14.375	83.91	17.74
500	1.4689	13.880	84.05	17.14
550	1.4669	13.298	84.2	16.42
600	1.4647	12.661	84.34	15.64
650	1.4625	11.995	84.47	14.82
700	1.4603	11.315	84.57	13.97
750	1.4584	10.637	84.62	13.13
800	1.4566	9.97	84.63	12.29
850	1.4546	9.323	84.6	11.47
900	1.4525	8.699	84.59	10.69
950	1.4504	8.103	84.6	9.94
1000	1.4482	7.537	84.59	9.23

the overall performance of the PSC. Moreover, a rise in the thickness of AL results in elevated series resistance, hence restricting current flow and negatively impacting total cell performance. The increased bulk recombination losses and decreased charge extraction PCE at increasing thicknesses increase this drop [28]. V_{oc} is a bit less sensitive to thickness variation than J_{SC} but still slightly reduced due to low carrier collection and recombination.

Figure 4(b) shows Quantum efficiency (QE) vs wavelength by varying AL thickness. As wavelength varies from 300 to 800nm corresponding to NIR and visible region where QE indicates the efficiency that can convert photons to charge carriers like electron and hole pairs that can contribute to current. Each curve indicates change in different thickness with respect to colours. QE drops at zero beyond 800nm as photons at this range don't have enough energy to be absorbed and generate charge carriers. As thickness increases which allows more photons to be absorbed by generation of charge carriers and boosting overall QE. Solar spectrum is most intense at QE peak which can be visible at 500-550nm for most thickness with high absorption efficiency. In UV region for all thickness obtained lower absorption efficiency as it is short wavelength due to reflection and recombination near the surface of the cell. Similarly, for longer wavelengths from 700 to 800nm reflects cut-off due to bandgap of AL as photons with energy which is below the bandgap cannot generate the electron hole pair. Investigating Table 3 indicates that stable FF highlights the stability of the charge transport layers (TiO_2 and Spiro-OMeTAD) despite variations in thickness.

Effect of Thickness in ETL, HTL and Absorber Layer for Model FTO/TiO_2/$MASnI_3$/Spiro OMeTAD

To evaluate the optimal performance of the model FTO/TIO_2/$MASnI_3$/SPIRO OMETAD, wherein $MASnI_3$ shows characteristics similar to those of lead halide perovskites, which are increasingly significant in this research

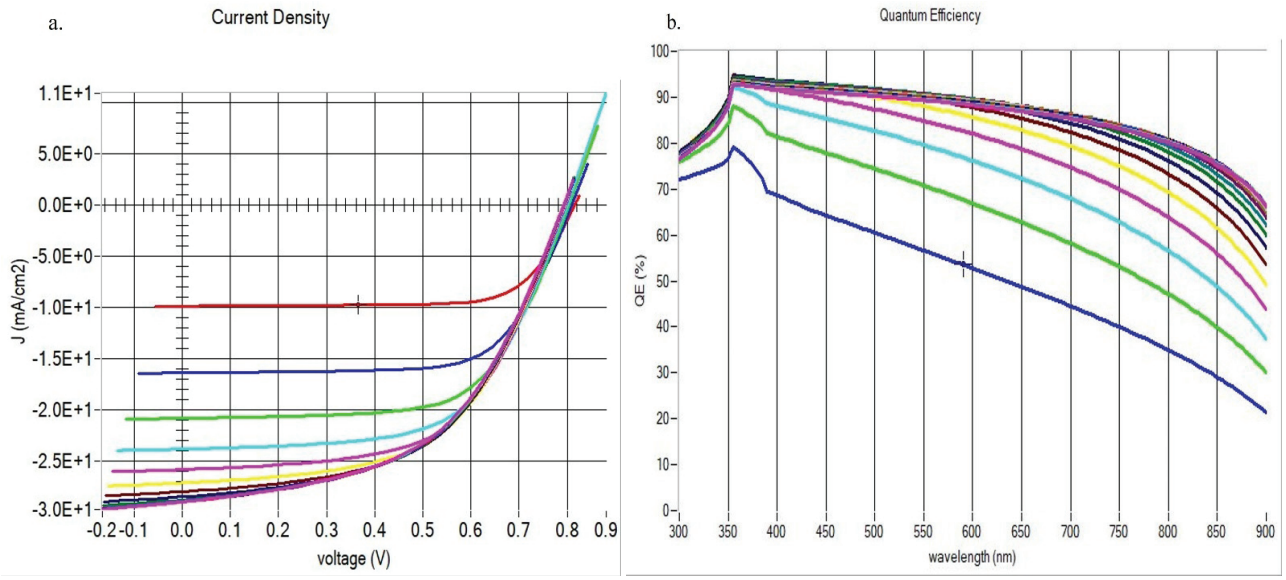

Figure 5. a. V-I curve and b. PCE curve for model FTO/TiO_2/$MASnI_3$/Spiro OMeTAD (obtained from SCAPS 1D simulator) (each color indicated different thickness of AL such as red for 50nm to maroon for 1000nm).

field. Figure 5(a) represents J-V curve for $MASnI_3$ based model where each curve represents different thickness of $MASnI_3$ by different color as similar to Figure 4(a). When thickness of $MASnI_3$ is less than 350nm, J_{SC} was low due to insufficient photon absorption as there is not enough light to be capture. Whereas, V_{oc} is stable but PCE is reduced due to limited electron-hole pair. Furthermore, when thickness was greater than 350nm FF and PCE decline due to recombination losses. Optimal thickness was at 350nm which was enough to capture most photons while maintaining efficient electron-hole pair. From the Table 4, demonstrate that at 350nm, maximum PCE was around 12%. Figure 5(b) is QE vs wavelength plot for $MASnI_3$ based model where, each curve represents different thickness with respect to color. Below 400nm obtained low QE due to parasitic absorption and reflection at Infront layer like FTO or TiO_2. High QE was obtained in the range of 400 to 600nm which indicates effective absorption of photons. Moreover, when QE reduces beyond 600nm and drop significantly after 700 to 800nm as it is explained in detailed in above case for $MAPbI_3$.

Figure 6 and 7 explains about function of thickness of AL on overall performance of PSCs. As V_{oc} peak at 1.473V approximately when its $MAPbI_3$ thickness is 200nm. High V_{oc} reflects excellent band alignment and has low defect density. Beyond 200nm, V_{oc} was reduce steadily due to recombination losses as explained in Figure 4 (a). similarly, V_{oc} for $MASnI_3$ starts at 0.816V and gradually drop as thickness increases due to its intrinsic instability and higher recombination losses which cause poor electron hole pairs. J_{SC} for $MAPbI_3$ reaches a peak at 14.985mA/cm^2 around 400nm and then slowly reduces as thickness increases due to challenge of transport of charge carrier. Whereas in $MASnI_3$ exhibits excellent light absorption at longer wavelength as already explained in Figure 4 (b) which leads in higher J_{SC}.

From the Figure 7 we can see that their efficiencies of $MAPbI_3$ and $MASnI_3$ where we notice that about

Table 4. Simulation results for model FTO/TiO_2/$MASnI_3$/Spiro OMeTAD(obtained from SCAPS 1D simulator)

t (nm)	V_{oc} (v)	J_{SC} (mA/cm^2)	FF (%)	PCE (%)
50	0.8162	9.856	72.63	5.84
100	0.8105	16.369	68.03	9.03
150	0.8050	20.8	63.82	10.69
200	0.8005	23.798	60.52	11.53
250	0.7974	25.8	57.77	11.89
300	0.7955	27.112	55.56	11.97
350	0.7941	28.455	53.95	12
400	0.794	28.748	52.87	11.95
450	0.794	28.902	51.78	11.88
500	0.794	28.97	51.58	11.87
550	0.794	28.972	51.53	11.87
600	0.7941	28.991	51.5	11.86
650	0.7941	28.989	51.47	11.85
700	0.7941	28.977	51.46	11.84
750	0.7942	28.967	51.44	11.83
800	0.7942	28.559	51.42	11.83
850	0.7942	28.955	51.4	11.82
900	0.7942	28.952	51.37	11.81
950	0.7942	28.95	51.33	11.8
1000	0.7942	28.948	51.3	11.79

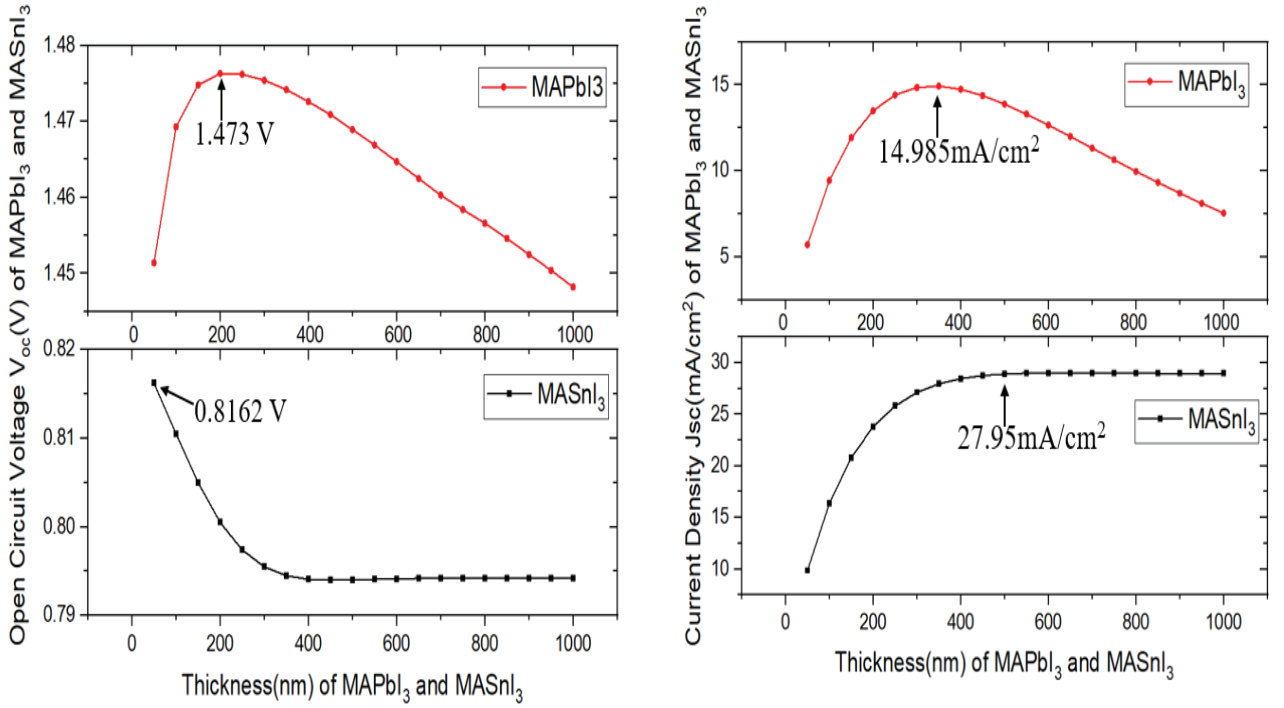

a. b.

Figure 6. Comparing simulation results of (a) V_{oc} and (b) J_{SC} of both models.

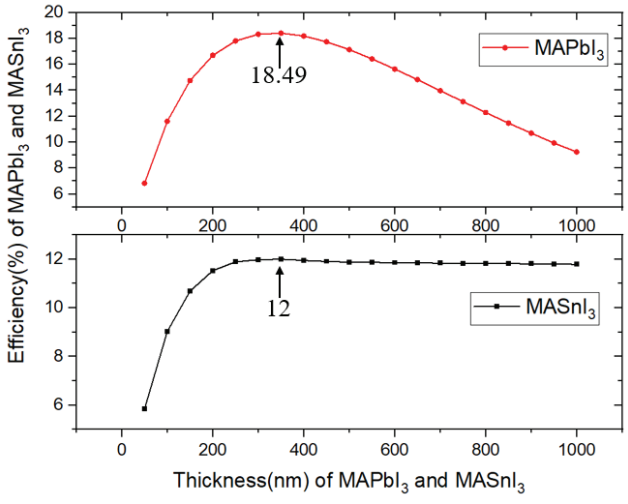

Figure 7. Comparing simulation result of efficiency of both models.

6% difference is observed in both devices. Efficiency of $MASnI_3$ based PSC can be improved by boosting bandgap with respect to HTL and change their film thickness.

Comparing Experimental Results with Simulation Results

To study and enhance the efficiency of $MAPbI_3$ solar cells, researchers assist with SCAPS 1D, a simulation tool that mirrors their functionality. These simulated results help in evaluating and intensifying the device's performance. Validating simulation outputs against experimental data ensures the precision of the model. Such an approach allows examination of the material's conduct in realistic scenarios, consequently augmenting comprehension of its real-world behaviour [29]. This study compares experimental and simulation methods in order to learn more about how $MAPbI_3$ photovoltaic cells work best and speed up the development of useful perovskite solar cells. This examination assesses the extent of agreement between the two forms of evaluation and identifies potential paths for enhancement [30]. Zhang et al. [31] made devices called $MAPbX_3$ (I, Br) and non-MAX (X = I, Br) and compared how well they worked with cells, as shown in Table 5 [31-35]. The SCAPS 1D simulation [31] demonstrated similar results.

Bouich et al. [36] fabricated $MASnI_3$ and compared with Table 6 to verify their cell performance. Antisolvent quenching improves solar cell perovskite films; however, no studies have examined its effect on $MASnI_3$ [36-40]. Based on $MASnI_3$ thin film structure and surface uniformity, antisolvent treatments were assessed. Optimized thermal annealing controls crystallization. Modifying the antisolvent improved supersaturation management. Results indicate that chlorobenzene and toluene minimize pinholes and enhance particle size. Toluene improved thin film shape and stability after four weeks in the dark with 60% humidity. Researcher used SCAPS-1D software to simulate how these antisolvents affect $MASnI_3$. To improved PCE by

Table 5. Compared simulation and experimental results of $MAPbI_3$

$MAPbI_3$	V_{oc} (v)	J_{SC} (mA/cm²)	FF (%)	PCE (%)
Simulation (present work)	1.4742	14.920	83.70	18.41
Simulation [32]	0.835	25.59	94.68	18.25
Experimental [31]	1.04	21.80	72	16.32
Experimental [33]	0.967	19.5	67.5	12.7
Simulation [34]	0.83	21.54	76.68	13.79
Simulation [35]	1.039	10	86.19	8.96

Table 6. Compared simulation and experimental results of $MASnI_3$

$MASnI_3$	V_{oc} (v)	J_{SC} (mA/cm²)	FF (%)	PCE (%)
Simulation	0.7941	28.455	53.95	12
Simulation [37]	0.95	15.2	61	9.7
Experimental [36]	0.90	13.69	84.01	10.44
Experimental [38]	0.81	21.9	67.6	11.99
Simulation [39]	0.95	15.2	61	9.2
Experimental [40]	0.931	14.86	63	8.74

5.11% when treated with chlorobenzene. Toluene-treated $MASnI_3$ devices improved PCE and stability by 9.44%.

While SCAPS-1D provides valuable insights into electrical characteristics under idealized conditions, the simulation does not fully capture real-world material imperfections such as grain boundaries, ion migration, or environmental degradation especially critical for Sn-based perovskites like $MASnI_3$, which are prone to oxidation. Additionally, the simulations assume perfect interfaces and uniform layer deposition, which may deviate from experimental fabrication outcomes. Future work involving experimental validation and degradation studies is essential to bridge the gap between simulated and practical performance.

CONCLUSION

The optimization of $MAPbI_3$ and lead free $MASnI_3$ based PSCs performance was investigated using SCAP 1D based simulation. The impact of various thickness of HTLs, ETLs and absorbers layers of perovskite was studied to get the best possible efficiency. It was observed that device with TiO_2 as ETL with thickness of 50nm, spiro OMeTAD as HTL with thickness of 100nm and finally $MAPbI_3$ and $MASnI_3$ with thickness of 350nm was seen with good efficiency which was compared with other researchers. By replacement of Pb with Sn has a significant impact on the perovskite material and by running the simulation for both devices we have obtained that $MASnI_3$ had lower performance than $MAPbI_3$ with V_{oc} = 0.7945V, J_{SC} = 27.95mA/cm², FF = 53.99%, and PCE = 12%, which are significantly lower than the PSC with $MAPbI_3$ (V_{oc} = 1.473V, J_{SC} = 14.985mA/cm², FF = 83.68% and PCE = 18.49%) except J_{SC}. We can see a significant differences of 6% in efficiency of both devices. However, in the case of Sn based perovskite we can increase the efficiency by improving the band gap alignment of material. The novelty of this study resides in its comprehensive comparison of $MASnI_3$ and $MAPbI_3$-based PSCs, focusing on performance optimization and material stability. Beyond present research, these results are the transfer of proposed, concrete pathways for new perovskites to power the large-scale green solutions of the future. This study lays foundational groundwork for improving $MASnI_3$-based PSCs, but future research should address intrinsic material instability, optimize alternative low-cost HTL/ETL materials, and explore encapsulation strategies to enhance operational stability under real-world conditions.

AUTHORSHIP CONTRIBUTIONS

Authors equally contributed to this work.

DATA AVAILABILITY STATEMENT

The authors confirm that the data that supports the findings of this study are available within the article. Raw data that support the finding of this study are available from the corresponding author, upon reasonable request.

CONFLICT OF INTEREST

The authors declared no potential conflicts of interest with respect to the research, authorship, and/or publication of this article.

ETHICS

There are no ethical issues with the publication of this manuscript.

STATEMENT ON THE USE OF ARTIFICIAL INTELLIGENCE

Artificial intelligence was not used in the preparation of the article.

REFERENCES

[1] National Renewable Energy Laboratory. Best research-cell efficiency chart [Internet]. Available at: https://www.nrel.gov/pv/cell-efficiency.html. Accessed November 16, 2026.

[2] Leela Devi V, Kuchhal P, de D, Sharma A, Kumar Shukla N, Aggarwal M. Machine learning-driven optimization of transport layers in $MAPbI_3$ perovskite solar cells for enhanced performance. IEEE Access 2024;12:179546–179565. [CrossRef]

[3] Kojima A, Teshima K, Shirai Y, Miyasaka T. Organometal halide perovskites as visible-light sensitizers for photovoltaic cells. J Am Chem Soc 2009;131:6050–6051. [CrossRef]

[4] Jena AK, Kulkarni A, Miyasaka T. Halide perovskite photovoltaics: Background, status, and future prospects. Chem Rev 2019;119:3036–3103. [CrossRef]

[5] Jiang Q, Zhao Y, Zhang X, Yang X, Chen Y, Chu Z, et al. Surface passivation of perovskite film for efficient solar cells. Nat Photonics 2019;13:460–466. [CrossRef]

[6] Husainat A, Ali W, Cofie P, Attia J, Fuller J. Simulation and analysis of methylammonium lead iodide ($CH_3NH_3PbI_3$) perovskite solar cell with Au contact using SCAPS 1D simulator. Am J Opt Photonics 2019;7:33. [CrossRef]

[7] Babayigit A, Ethirajan A, Muller M, Conings B. Toxicity of organometal halide perovskite solar cells. Nat Mater 2016;15:247–251. [CrossRef]

[8] Frost JM, Butler KT, Brivio F, Hendon CH, van Schilfgaarde M, Walsh A. Atomistic origins of high-performance in hybrid halide perovskite solar cells. Nano Lett 2014;14:2584–2590. [CrossRef]

[9] Maqsood A, Abid MI, Kamran M, Turzyński M, Tlija M, Ghith E. Optimization of lead-free Sn-based perovskite solar cells using SCAPS-1D simulation techniques. Preprints 2024. [CrossRef]

[10] Shoab M, Aslam Z, Zulfequar M, Khan F. Numerical interface optimization of lead-free perovskite solar cells (CH3NH3SnI3) for 30% photo-conversion efficiency using SCAPS-1D. Mater 2024;4:100200. [CrossRef]

[11] Afridi K, Noman M, Jan ST. Evaluating the influence of novel charge transport materials on the photovoltaic properties of MASnI3 solar cells through SCAPS-1D modelling. R Soc Open Sci 2024;11:231202. [CrossRef]

[12] Park HJ, Son H, Jeong BS. SCAPS-1D simulation for device optimization to improve efficiency in lead-free CsSnI3 perovskite solar cells. Inorganics 2024;12. [CrossRef]

[13] Toygun Ş, Köneçoğlu G, Kalpaklı Y. General principles of sol-gel. Sigma J Eng Nat Sci 2013;31:456–476.

[14] Shankar G, Kumar P, Pradhan B. All-perovskite two-terminal tandem solar cell with 32.3% efficiency by numerical simulation. Mater Today Sustain 2022;20:100241. [CrossRef]

[15] Kılıç HŞ, Yiğit Gezgin S, Candan İ, Baturay Ş. Modelling of the solar cell based on Cu2SnS3 thin film produced by spray pyrolysis. Middle East J Sci 2022;8:64–76. [CrossRef]

[16] Zhang Y, Li L, Su H, Huang W, Dong X. Binary metal oxide: Advanced energy storage materials in supercapacitors. J Mater Chem A 2015;3:43–59. [CrossRef]

[17] Kim HS, Im SH, Park NG. Organolead halide perovskite: New horizons in solar cell research. J Phys Chem C 2014;118:5615–5625. [CrossRef]

[18] Sarukura N, Murakami H, Estacio E, Ono S, El Ouenzerfi R, Cadatal M, et al. Proposed design principle of fluoride-based materials for deep ultraviolet light emitting devices. Opt Mater 2007;30:15–17.

[19] Liu F, Zhu J, Wei J, Li Y, Lv M, Yang S, et al. Numerical simulation: Toward the design of high-efficiency planar perovskite solar cells. Appl Phys Lett 2014;104:253508–253508. [CrossRef]

[20] Lee M, Teuscher J, Miyasaka T, Murakami T, Im J-H. Efficient hybrid solar cells based on meso-superstructured organometal halide perovskites. Science 2012;338.

[21] Jeon NJ, Lee HG, Kim YC, Seo J, Noh JH, Lee J, et al. o-Methoxy substituents in Spiro-OMeTAD for efficient inorganic-organic hybrid perovskite solar cells. J Am Chem Soc 2014;136:7837–7840. [CrossRef]

[22] Baig F, Khattak YH, Marí B, Beg S, Ahmed A, Khan K. Efficiency enhancement of CH3NH3SnI3 solar cells by device modeling. J Electron Mater 2018;47:5275–5282. [CrossRef]

[23] Azri F, Meftah A, Sengouga N, Meftah A. Electron and hole transport layers optimization by numerical simulation of a perovskite solar cell. Sol Energy 2019;181:372–378. [CrossRef]

[24] Minemoto and M. Murata T. Impact of work function of back contact of perovskite solar cells without hole transport material analyzed by device simulation. Curr Appl Phys 2014;14:1428–1433.

[25] Raj A, Kumar M, Kumar A, Laref A, Singh K, Sharma S, et al. Effect of doping engineering in TiO2 electron transport layer on photovoltaic performance of perovskite solar cells. Mater Lett 2022;313:131692. [CrossRef]

[26] Nugraha H, Dharma C, Jaafar J, Widiastuti N, Matsuyama H, Rajabsadeh S, et al. A review of titanium dioxide (TiO2)-based photocatalyst for oilfield-produced water treatment. Membranes 2022;12. [CrossRef]

[27] Hatamvand M, Vivo P, Liu M, Tayyab M, Dastan D, Cai X, et al. The role of different dopants of Spiro-OMeTAD hole transport material on the stability of perovskite solar cells: A mini review. Vacuum 2023;214:112076. [CrossRef]

[28] Aliaghayee M. Optimization of the perovskite solar cell design with layer thickness engineering for improving the photovoltaic response using SCAPS-1D. J Electron Mater 2023;52:2475–2491. [CrossRef]

[29] Raoui Y, Ez-Zahraouy H, Ahmad S, Kazim S, Tahiri N, Omar EB. Performance analysis of MAPbI3 based perovskite solar cells employing diverse charge selective contacts: Simulation study. Sol Energy 2019;193C:948–955. [CrossRef]

[30] Sivakumar N, Saha S, Madaka R, Bandaru N, Rath JK. Investigation on the structural, spectral, and optical properties of MAPbI3.H2O and MAPbI3 perovskite crystals for photovoltaic cells. J Mater Sci Mater Electron 2023;34. [CrossRef]

[31] Zhang T, Guo N, Li G, Qian X, Li L, Zhao Y. A general non-CH3NH3X (X = I, Br) one-step deposition of CH3NH3PbX3 perovskite for high performance solar cells. J Mater Chem A 2016;4:3245–3248. [CrossRef]

[32] Belarbi M, Zeggai O, Louhibi-Fasla S. Numerical study of methylammonium lead iodide perovskite solar cells using SCAPS-1D simulation program. First Maghrebian Conf Renew Energ Their Appl 2022;51:2115–2119. [CrossRef]

[33] Casaluci S, Cinà L, Pockett A, Kubiak PS, Niemann RG, Reale A, et al. A simple approach for the fabrication of perovskite solar cells in air. J Power Sources 2015;297:504–510. [CrossRef]

[34] Son C, Son H, Jeong B-S. Enhanced conversion efficiency in MAPbI3 perovskite solar cells through parameters optimization via SCAPS-1D simulation. Appl Sci 2024;14. [CrossRef]

[35] Ul Rehman A, Ahmed HH, Bilal M, Afzal S. A comprehensive SCAPS-1D performance evaluation of MAPbX3-based perovskite solar cells (PSCs). Eurasian J Sci Technol 2025;5:88–105.

[36] Bouich A, Marí Guaita J, Marí Soucase B, Palacios P. Manufacture of high-efficiency and stable lead-free solar cells through antisolvent quenching engineering. Nanomaterials 2022;12. [CrossRef]

[37] Benami A, Ouslimane T, Et-Taya L, Sohani A. Comparison of the effects of ZnO and TiO2 on the performance of perovskite solar cells via SCAPS-1D software package. J Nano Electron Phys 2022;14:01033. [CrossRef]

[38] Moyez S, Roy SA. Dual-step thermal engineering technique: A new approach for fabrication of efficient CH3NH3PbI3-based perovskite solar cell in open air condition. Sol Energy Mater Sol Cells 2018;185:145–152. [CrossRef]

[39] Zhang P, Xiong J, Chen WH, Du P, Song L. Air-processed MAPbI3 perovskite solar cells achieve 20.87% efficiency and excellent bending resistance enabled via a polymer dual-passivation strategy. Dalton Trans 2023;52:15974–15985. [CrossRef]

[40] Kang R, Yeo JS, Lee HJ, Lee S, Kang M, Myoung N, et al. Exploration of fabrication methods for planar CH3NH3PbI3 perovskite solar cells. Nano Energy 2016;27:175–184. [CrossRef]